nature communications

Article

https://doi.org/10.1038/s41467-026-68605-y

Expanding the payload scope in antibody-drug conjugates by delivery of hydroxy-containing drugs through self-immolative phosphoramidates

Received: 27 November 2024

Accepted: 13 January 2026

Published online: 20 January 2026

Check for updates

Philipp Ochtrop[1], Anil P. Jagtap[1], Jan G. Felber[1], Simon Vogt[1], Sarah Herterich[1], Isabelle Mai[1], Philipp Cyprys[1], Saskia Schmitt[1], Sarah Payer[1], Annabel Kitowski[1], Swetlana Wunder[1], Paul Machui[1], Julia Brandmeier[1], Natascia Leonardi[1], Elizaveta Poliak[1], Christian P. R. Hackenberger[2,3], Olivier Marcq[1], Dominik Schumacher[1], Jonas Helma[1], Annette M. Vogl[1] & Marc-André Kasper[1]

Despite recent advances in targeted drug delivery, approved Antibody-Drug-Conjugates (ADCs) are still limited by the delivery of a restricted set of payloads with limited modes of action (MOA). Versatile linkers, applicable to functional groups prevalent across diverse pharmacophores are needed to expand this space. We present phosphoramidate-based self-immolative linker-units that facilitate stable attachment in serum and traceless drug release in the target cell of aliphatic and aromatic alcohols. Studies with camptothecins show that stability and release are tunable and that various intracellular trigger events can be exploited to ensure traceless drug delivery. Superior stability, in vivo efficacy, and pharmacokinetics (PK) compared to approved camptothecin ADCs are demonstrated. Moreover, we report targeted delivery of 10 different hydroxy-containing cytotoxins with different intracellular MOAs. In vivo studies with gemcitabine show excellent PK and efficacy, unlocking gemcitabine's full potential and illustrating the ability of the phosphoramidate-based linker system to expand the payload space for ADCs.

Targeted drug delivery for the treatment of malignant diseases holds great promise in reducing undesired side effects while increasing efficacy by precisely hitting cancer cells[1]. Most prominently, antibodies conjugated to highly potent cytotoxic drugs, a modality known as antibody-drug conjugates (ADCs), have been utilized as targeting vehicles[2,3]. The pace of more new ADCs entering clinical trials and receiving FDA approval has accelerated over the past decade, underlining the benefits of targeted drug delivery for patients[4]. Still, challenges remain to be solved, such as chemotherapy-like toxicities, lack of efficacy when applied as monotherapy and, eventually, acquired resistance[5].

The potency and mode of action (MOA) of the cytotoxic payload that is being delivered is considered as one of the major drivers of these shortcomings[6]. With a small repertoire of only three MOAs in approved ADCs, namely tubulin-inhibition, topoisomerase-I (TOP1)-inhibition and DNA -damaging, it is anticipated that MOA diversification will be a key factor in the development of next generation targeted cancer therapeutics[7]. Another Achilles' heel that has been identified in the current generation of ADCs is the linker between antibody and drug. Ongoing research efforts aim to improve linker associated limitations such as premature drug loss[8], unspecific uptake[9,10] and undesired aggregation[11].

[1]Tubulis GmbH, IZB, Planegg-Martinsried, Germany. [2]Chemical Biology Department, Leibniz-Forschungsinstitut für Molekulare Pharmakologie (FMP), Berlin, Germany. [3]Department of Chemistry, Humboldt Universität zu Berlin, Berlin, Germany. e-mail: marc.kasper@tubulis.com

On top of that, linker design determines the cleavability and drug release at the targeted location. In particular, efficient, traceless drug release after receptor-mediated uptake can be crucial for the intracellular function of the payload[12] and for its permeability, which allows effective eradication of tumors with heterogenous expression of the antibody's target via the bystander effect[13,14]. Hence, cleavable linker systems are required that provide a stable attachment of a payload via one of its functional groups during circulation and, importantly, simultaneously allow for traceless release of this functional group upon uptake into the targeted cell. Cleavable linker systems usually consist of a release unit that is activated by an intracellular trigger event, and a self-immolative moiety that subsequently liberates the unmodified functional group[1,15]. Commonly exploited trigger events include a variety of intracellular or intra-lysosomal conditions such as acidic and reductive environment or specific enzymatic activities from esterases[16], proteases[17], glycosidases[18], phosphatases[19], reductases[20], or sulfatases[21]. Recent developments in the field focused on enhancing the stability and efficacy of widely used cathepsin B cleavable linkers by tackling the premature payload release through unspecific cleavage of the VC peptide. Especially the introduction of exo-cleavable[22], tandem-cleavable[23] or carboxylesterase resistant linker[24] showcase the impact of linker design on ADC stability and efficacy.

Such cleavable linkers have been designed for the attachment of different functional groups on payloads including primary-[25], secondary-[26], tertiary- and heteroaryl-amines[27], thiols, amides[28], ortho-quinones[29] and alcohols[30]. In particular, hydroxyl linkages are attractive since this functionality is frequently present in synthetic small molecule drugs and natural product derivatives[31]. However, based on their chemical environment, hydroxyl groups can differ tremendously in steric accessibility and pKa, ranging from 7 (phenols) to 16 (aliphatic alcohols). This broad scope poses a challenge for the design of broadly applicable linker systems that allow for both stable attachment and traceless release of chemically distinct alcohols. Available linker systems for alcohol attachment rely on carbamates[32], carbonates[33], esters[34], phosphates, pyrophosphates[35], 1,6-benzylamines[36], hemiaminals[37,38], disulfides[20,39], or methylene carbamates[30]. DXd represents one of the clinically successful examples in which a primary alcohol has been stably linked and its sufficient release can be ensured via a cleavable hemiaminal structure[40,41]. However, the broad applicability of hemiaminals to hydroxy functions of different pKa remains to be shown. Therefore, none of the functional groups that have been used so far for hydroxyl group attachment combine broad applicability, stability in serum and efficient traceless release.

To address these limitations, we took inspiration from the clinically validated ProTide technology[42], a prodrug system that has been developed to mask hydrophilicity of nucleoside-like drug molecules to enhance cell permeability[43]. This approach has yielded three FDA-approved antiviral drugs, sofosbuvir[44], tenofovir alafenamide[45], and remdesivir[46], that have become blockbuster therapeutics, underscoring the ProTide strategy's success in antiviral therapy and its growing promise in oncology[47–49]. Continued advancements in ProTide chemistry, including applications beyond traditional nucleoside analogs, further highlight its versatility[50]. After passive membrane diffusion, these prodrugs are activated via esterase cleavage of an amino acid ester followed by self-immolation via a 5-membered cyclization, release of a sacrificial phenol and finally, enzymatical release of the (phosphorylated) nucleoside analog (Fig. 1a).

In this work, we redesign the central phosphorous core of the phosphoramidate moiety by introducing a conjugation handle to one of the three *P*-substituents that can form a covalent bond with a targeting moiety like an antibody. Therby we transform a prodrug system into a targeted drug delivery technology. Exploiting the fact that ProTides liberate an aromatic- and an aliphatic alcohol intracellularly, we extend this concept to create a linker-technology capable of releasing not only nucleoside analogs but delivering a broad spectrum of aliphatic- and aromatic alcohols (Fig. 1b). In contrast to the earlier described nucleoside prodrugs which are restricted to esterase cleavage after passive uptake into the cytosol[42], the release from our phosphoramidate-based targeted drug delivery system can be initiated by various intracellular and endosomal triggers including esterases, proteases, glucoronidases and reductive conditions due to the uptake mechanism via receptor-mediated endocytosis.

Results and discussion

Establishment of phosphorus-based self-immolative handles for the targeted delivery of aromatic alcohols exemplified with SN38

To start our endeavors, we chose the TOP1-inhibitor SN38, the active pharmaceutical ingredient (API) of the clinically approved ADC sacituzumab govitecan (SG, Trodelvy), as our first model drug[51]. Guided by previous experience with unsaturated ethynyl-[52] and vinyl-

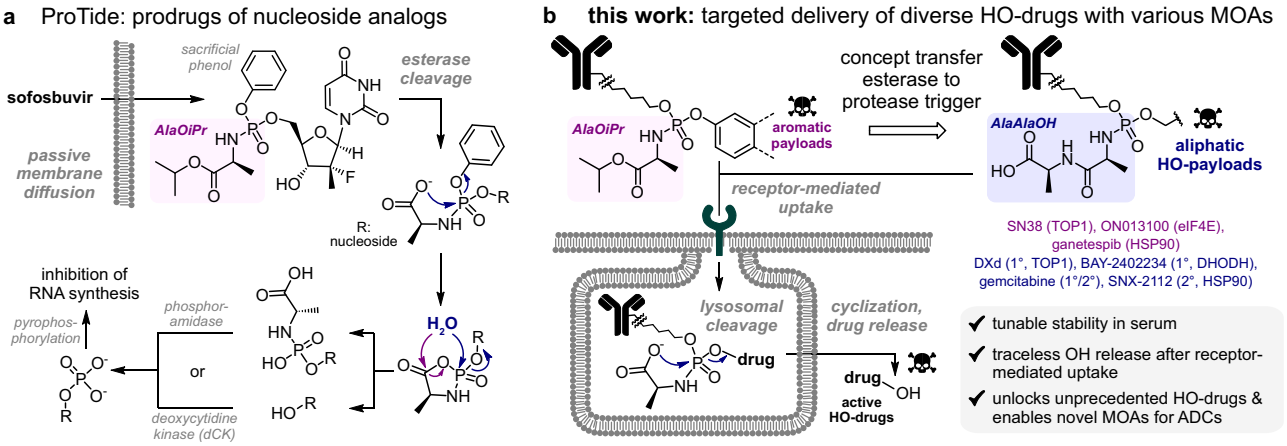

Fig. 1 | Structural comparison between ProTide prodrugs and development of the phosphoramidate linker moiety for traceless release of aromatic- and aliphatic alcohols in targeted drug delivery. a Mechanism of ProTide release after passive diffusion into the cytosol[42]. AlaOiPr release handle is highlighted with pink background. **b** Re-design of phosphoramidates as linkers for targeted drug delivery. Phosphoramidate-based structures and proposed mechanism for intracellular release of aromatic and aliphatic drugs via the linker systems described herein. AlaOiPr-(esterase trigger) is highlighted with pink background and AlaAlaOH-(protease trigger) is highlighted with purple background. Representation of the aromatic and aliphatic alcohols with MOAs that have been used as ADC payloads in the current work.

https://doi.org/10.1038/s41467-026-68605-y

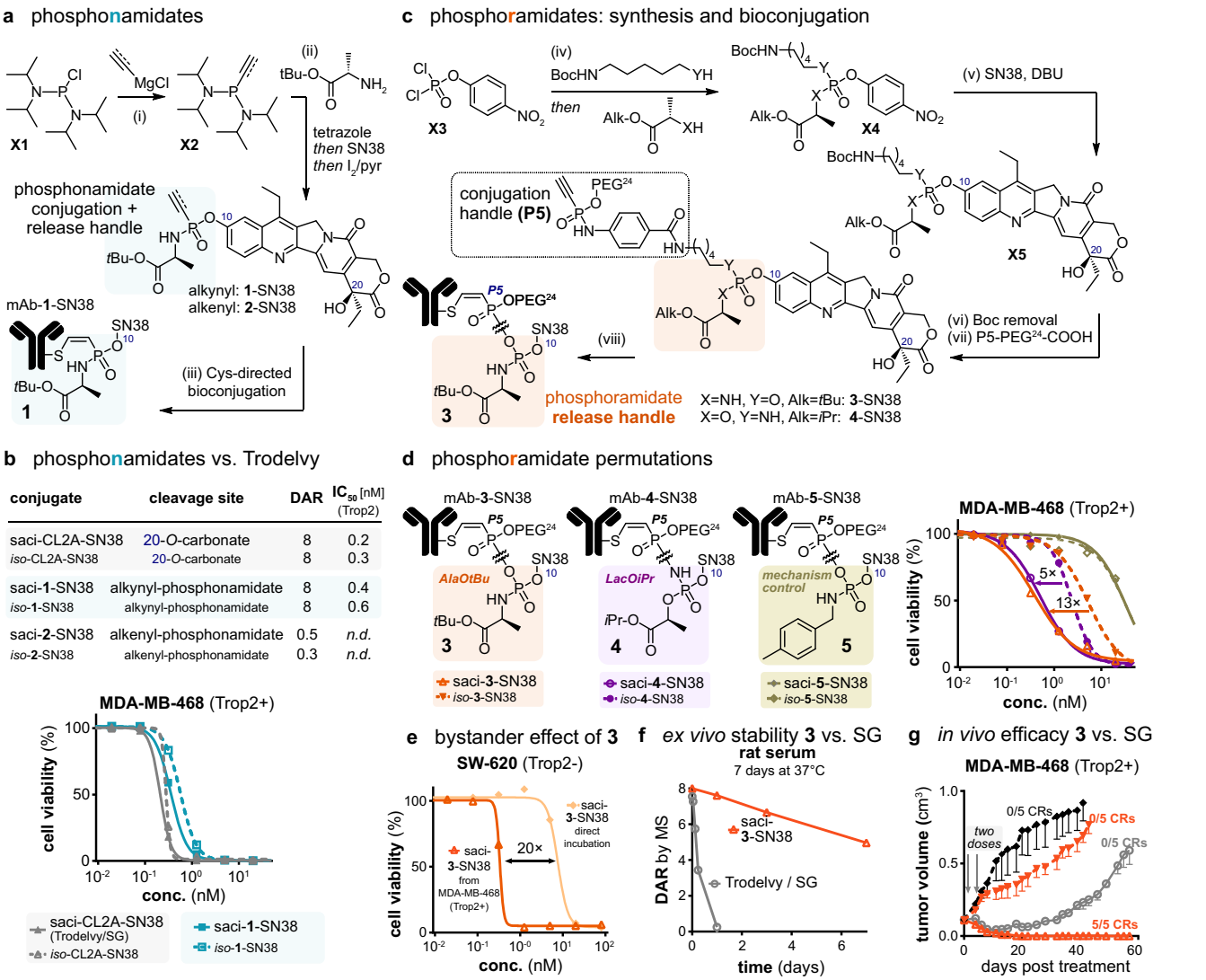

Fig. 2 | Evaluation of ADCs with phosphorus-based self-immolative linkers and aromatic alcohols, exemplified with SN38. a Synthesis of phosphonamidate-based linker-payloads **1**/**2**-SN38 (phosphonamidate structure is highlighted with turquoise background): (i) ethynyl or vinyl magnesium bromide, THF; (ii) tetrazole, then SN38, tetrazole, MeCN/THF, then I_2, pyridine; (iii) Sacituzumab (saci) or Isotype (iso) mAb, TCEP, **1**/**2**-SN38, 15 h at pH 8.3. **b** Evaluation of SG (Trodelvy), highlighted in gray, and sacituzumab (saci/anti-Trop2)-**1**/**2**SN38, in comparison to isotype controls. Anti-proliferative dose-response curves for saci-**1**-SN38 (solid, turquoise), SG (solid, gray) and isotype ADCs (dashed) on MDA-MB-468 cells (Trop2 +). **c** Synthesis of phosphoramidate-based linker-payloads **3**/**4**-SN38 (the phosphoramidate structure is highlighted with orange background). (iv) alanine *tert*-butyl ester or isopropyl lactate, then *N*Boc 1,5-diaminopentane or *N*Boc-aminopentanol, Et_3N, THF; (v) SN38, DBU, DMSO; vi) TFA, CH_2Cl_2; vii) P5(PEG24)-COOH, PyBOP, DIPEA, DMSO. (viii) Sacituzumab (saci/anti-Trop2) or brentuximab (bren/anti-CD30), TCEP, **3**/**4**-SN38, pH 8.3, 15 h. **d** Structure and cytotoxicity of saci-**3**/**4**-SN38 and the non-cleavable saci-**5**-SN38 against their respective isotype ADCs on MDA-MB-468 (Trop2 +). The alanine-O*tBu* release handle is highlighted with an orange background, the iPr-lactate release handle is highlighted with a purple background and the non-cleavable substituent highlighted with an ocher. Anti-proliferative dose response curves for saci-ADCs (solid) and isotype ADCs (dashed) on MDA-MB-468 cells (Trop2 +). Graphs show mean, $n = 2$. **e** Bystander killing: SW-620 cells (Trop2-) treated with increasing concentrations of Saci-**3**-SN38 (light orange) or with the supernatant of MDA-MB-468 cells (Trop2 +) (orange) that have been pre-treated with increasing concentrations of saci-**3**-SN38. Dose-response curves show the direct antiproliferative effect or the indirect effect (bystander) of released payload in the supernatant on SW-620. Graphs show mean, $n = 2$. **f** Rat serum stability: DAR measured by mass spectrometry of SG (gray) or saci-**3**-SN38 (orange) after incubation for up to 7 days in rat serum at 37 °C. Graphs show mean, $n = 2$. **g** In vivo efficacy evaluation of saci-**3**-SN38 (orange open upward-pointing triangle), iso-**3**-SN38 (orange filled downward-pointing triangle), SG (gray open circle) and vehicle (black filled diamond). Female CB17-SCID mice have been implanted with cell-culture-derived xenograft model based on MDA-MB-468 cells in matrigel (corresponding in vitro effect for this cell line is shown in (**b**, **d**). Treatment started once tumor volumes reached 0.1–0.15 cm^3. Mice ($n = 5$ per group) were treated at day 0 and day 4 with 10 mg/kg of the ADCs. Shown is the Mean ± SEM of the 5 animals.

phosphonamidate[53]-based linker technologies, we designed linker structures **1** and **2** for cysteine-selective antibody conjugation and attached SN38 via its aromatic 10-hydroxyl group as *O*-substituent of the phosphonamidates. In this design, the alaninyl *tert*-butyl ester at the phosphorus *N*-substituent is supposed to act as release trigger. Upon intracellular *tert*-butyl ester hydrolysis, cyclization via a 5-membered intermediate could lead to a traceless release of unmodified SN38 via a similar mechanism as described for the phenol in Fig. 1a. Synthesis of **1** and **2** was performed as outlined in Fig. 2a (See SI for detailed information). Conjugation of **1**-SN38 to sacituzumab and an isotype antibody delivered homogenous ADCs with a drug-to-antibody ratio (DAR) of 8, while a conjugation with **2**-SN38 was not suitable to produce ADCs with DAR higher than 0.5. These observations reflect the previously reported reactivity differences between

https://doi.org/10.1038/s41467-026-68605-y

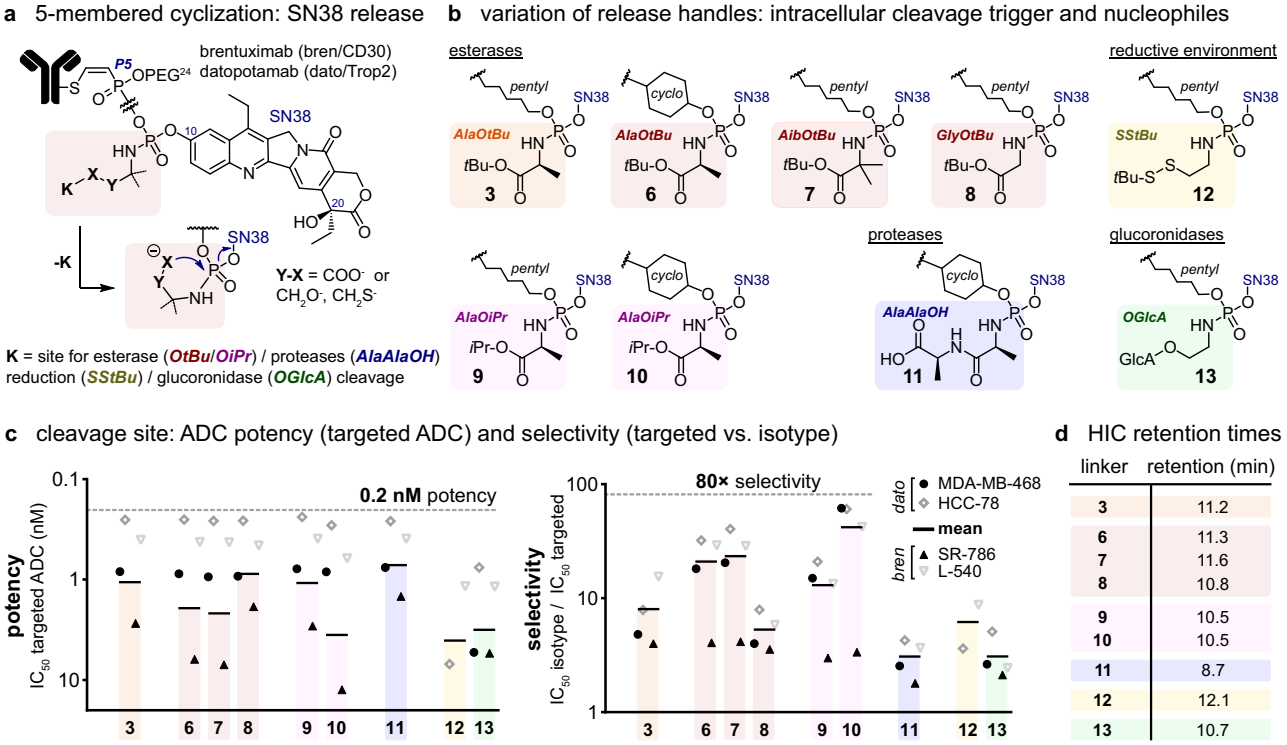

Fig. 3 | Variation of the phosphoramidate-based release handles. a DAR8 ADCs from brentuximab (bren/anti-CD30) and datopotamab (dato/anti-Trop2) using SN38 and various phosphoramidate-based self-immolative release handles (highlighted with red background), amenable for esterase-, protease-, reductase-, or glucoronidase-initiated release by 5-membered cyclization. **b** Chemical structures for various phosphoramidate-based side chains applied in linker **3** and **6**-**13**. Alanine *tert*-butyl ester release handle is highlighted with orange background, variations of alanine *tert*-butyl ester release handles are highlighted with red background, alanine *iso*-propyl ester release handles are highlighted with light pink background, protease cleavable di-alanine release handle is highlighted with purple background, reductive cleavable release handle is highlighted with yellow background and glucuronidase cleavable release handle is highlighted with green background. **c** Potency and selectivity of the different ADC constructs for the targeted cell line. Bren-ADCs were tested on L-540 and SR-786 cells (CD30 +), dato-ADCs were tested on HCC-78 and MDA-MB-468 cells (Trop2 +), while they served as isotypes vice versa. The ADC selectivity is plotted as the ratio of IC_{50} isotype/IC_{50} targeted ADC. The absolute potencies of the bren-/dato-ADCs are plotted for their target-positive cell lines. Orange columns refer to alanine *tert*-butyl ester release handle, red columns refer to variations of alanine *tert*-butyl ester release handles, light pink columns refer to alanine *iso*-propyl ester release handles, purple columns refer to di-alanine release handle, yellow columns refer to reductive cleavable release handle and green columns refer to glucuronidase cleavable release handle. The black bars show the mean values each for the four cell lines (targeted via two distinct receptor-antibody-pairs) and serve as orientation to compare the different linker structures. Dose-response curves are shown in Fig. S2. **d** Hydrophilicity of the DAR8 ADCs for the dato conjugates, derived from the retention time in hydrophobic interaction chromatography (HIC). The colored shades refer to the various release handles. Orange for alanine *tert*-butyl ester, red for variations of alanine *tert*-butyl esters, light pink for alanine *iso*-propyl esters, purple for di-alanine, yellow for reductive cleavable release handle and green for glucuronidase cleavable release handle.

ethynyl and vinyl-phosphonamidates with cysteines and consequently disqualified **2**-SN38 as an efficient drug-linker for SN38[53].

Next, we wanted to explore the properties of the linker systems **1** and **2** and compare them with the established linker system of SG (CL2A-SN38). In the linker (CL2A-SN38) of SG, SN38 is attached at its tertiary 20-hydroxyl group via a carbonate moiety (Fig. 3a). This linker has been designed to rapidly hydrolyze under physiological conditions. As previously reported[54] and confirmed by our in vitro cell culture assays, this lability leads to extracellular release of SN38, causing cell killing also of non-targeted cells with isotype ADCs that are not actively internalized. Consequently, the IC_{50} of targeted vs. isotype ADC in cell viability experiments with multiple days of incubation are highly similar (0.2 nM versus 0.3 nM, Fig. 2b). Previously reported efforts to generate a serum stable linker, in which SN38 is attached via a carbamate to the aromatic 10-hydroxyl group, failed to show efficacy due to insufficient intracellular release of SN38 as indicated by higher IC_{50} than for SN38 as free drug[33]. These two scenarios observed for SN38-containing linker systems inspired us to employ in vitro proliferation assays with isotype versus targeted ADCs as a reliable, close-to-application readout to optimize our linker system for stability and release efficiency. For this reason, we analyzed the ratio of IC_{50} from isotype- over targeted ADC as measure for linkage stability, and absolute IC_{50} of the targeted ADC as measure for effective release. We subjected sacituzumab-**1**-SN38 to in vitro cytotoxicity assays with the Trop2-positive MDA-MB-468 cancer cell line and observed almost identical IC_{50} values for targeted and isotype ADCs of 0.4 and 0.6 nM, respectively, indicating insufficient stability under cell culture conditions, similar as observed for SG (Fig. 2b). This instability stands in strong contrast to previously reported *O*-alkyl ethynylphosphonamidate-based ADCs that were shown to be highly stable under physiological conditions, in vitro and even in vivo. We attribute the lability of **1**-SN38 to the strong leaving group character of the aromatic SN38, which leads to fast hydrolysis of the phosphonamidate under assay conditions.

To stabilize the linker system against hydrolysis, we envisioned exchanging the carbon at the phosphorous core to oxygen and introducing a short amino pentyl linker as second *O*-substituent while keeping the *N*-alanine *tert*-butyl ester as release handle. By attaching a suitable antibody conjugation handle such as ethynylphosphonamidates (P5-conjugation)[12,55], this resulted in phosphoramidate-based linker-payloads **3** and its variations **4** and **5**. In linker **4** *O*- and *N*-substituted linker and release handle are swapped, while in **5** the release handle is exchanged to a non-cleavable 4-methylbenzyl group. Linkers **3**-**5** were synthesized as outlined in Fig. 2c (See SI for detailed

information) and proved to be superior to **1**-SN38, since **3**-**4**-SN38, conjugated to sacituzumab, exhibited strong anti-proliferative activity with a favorable potency window between targeted and isotype ADC (Fig. 2d). An IC_{50} of 0.4 nM and a 13-fold difference for the Trop2-targeted ADC saci-**3**-SN38 vs. the isotype ADC indicates a more stable SN38 conjugation to the mAb compared to SG or **1**-SN38, while allowing an efficient release of the drug after receptor-mediated cellular uptake. A similar behavior was observed for saci-**4**-SN38. However, since the selectivity window was slightly lower (5-fold) we decided to continue our studies using linker **3**. Interestingly, targeted ADCs based on the non-cleavable control **5**-SN38, lacking an intracellular release trigger, only showed an anti-proliferative effect at the highest concentration in vitro. These results indicate that phosphoramidate-based linker systems **3** and **4** provide a stable connection of SN38 via its aromatic alcohol which can be cleaved intracellularly, involving enzyme-mediated hydrolysis of the ester in the release handle. Next, we set out to investigate the bystander effect of saci-**3**-SN38[14]. As shown in Fig. 2e, saci-**3**-SN38 exhibits strong bystander killing of Trop2- cells after supernatant transfer from Trop2+ cells preincubated with ADC, but only very low direct cell killing of the target-negative cells. Since traceless payload release from the linker has been described as a key requirement for bystander activity, this data further indicates efficient, traceless SN38 release after receptor-mediated uptake from **3**-SN38[56].

We then set out to compare **3**-SN38 head-to-head with SG to evaluate whether phosphoramidates could improve the established Cl2A linker in SG. We confirmed target selectivity for saci-**3**-SN38 in vitro on a larger panel of cell lines, in contrast to CL2A-SN38 that proved to be unselective, (Fig. S1) and observed improved rat serum stability of saci-**3**-SN38 with more than 50% intact ADC after 7 days of incubation (Fig. 2f). In contrast, SG lost almost 100% of conjugated drug already after 24 hours, mainly caused by carbonate hydrolysis. Since tumor-target specificity of SG has been demonstrated in vivo, contrary to the in vitro observations[54], we compared both linker-payloads head-to-head in an in vivo efficacy experiment (Fig. 2g). Here, Trop2+ tumor bearing mice were treated twice (day 0 and day 4) with 10 mg/kg of saci-**3**-SN38, iso-**3**-SN38, SG or vehicle. We observed a superior efficacy with complete responses for saci-**3**-SN38 in all mice while SG only led to delayed tumor growth and iso-**3**-SN38 showed no clear responses. We attribute this enhanced anti-cancer activity to improved linker stability, as previously reported in other systems[55,57], ensuring a higher tumor exposure to SN38. In addition, we tested saci-**3**-SN38 and SG on a panel of healthy human primary cells to assess differences of the linker structures on the undesired effect on normal tissue (Fig. S1c). On all of the tested healthy cells, saci-**3**-SN38 had significantly less effect compared to SG, suggesting not only a higher anti-tumor efficacy of the linker systems described herein but also reduced effect on healthy tissue and thereby a broader therapeutic window.

Linker stability tuning and combination with different release triggers

Encouraged by reports on structural optimization of ProTides[42], we set out to tune potency and stability of our phosphoramidate-based linker system by synthesizing derivatives of linker **3** attached to SN38. For evaluation, we conjugated the resulting linker-payloads to two different antibodies, targeting the cell-surface cancer antigens Trop2 and CD30, which were characterized for potency (IC_{50} targeted ADC) and selectivity (ratio IC_{50} isotype/targeted ADC) on two target-positive cell lines for each ADC (Fig. 3a and Fig. S2). To increase electron density at P, we synthesized linker **6**, in which the primary pentyl *O*-substituent of linker **3** is exchanged to a secondary cyclohexyl *O*-substituent, and linker **7**, in which we introduced an additional methyl group at the amino acid alpha carbon. We also aimed to reduce electron density at the phosphorus by exchanging the alanine in linker **3** to a glycine in linker **8** (Fig. 3b). We observed that an increase in electron density in linkers **6** and **7** lead to a larger difference between targeted and isotype ADCs, whereas linker **8**, possessing less electron density at the phosphorus, showed a decreased window (Fig. 3c). At the same time, we observed slightly reduced median potencies for the ADCs based on **6**-SN38 and **7**-SN38 compared to **3**-SN38 and **8**-SN38, which might be attributed to steric hindrance leading to either reduced esterase activity or reduced cyclization rates between the liberated carboxylic acid and the central phosphorus atom. To further study this, we exchanged the esterase cleavable *tert*-butyl ester in the derivatives **3** and **6** to isopropyl esters in linkers **9** and **10**, following previous reports on ProTides that *tert*-butyl esters are less efficiently cleaved by esterases[58]. This trend could be confirmed with esterase cleavage assays on *N*-Acetyl-Cysteine adducts of the isolated linker payloads **3**-, **9**- and **10**-SN38, showing a faster release of the payload from the isopropyl esters **9** and **10** compared to the tert-butyl ester in **3** (Fig. S3). Interestingly, this change did not have an effect on the median potency on the targeted cell line but the selectivity slightly increased from *tert*-butyl- to isopropyl esters in both cases.

The cleavable phosphoramidate-based linkers described to this point are all designed to be activated analogously by esterase-mediated cleavage of the respective amino-acid ester. Next, we wanted to explore if the cleavage can also be initiated via alternative release triggers that are commonly applied in antibody-mediated drug-delivery[2]. In contrast to prodrugs, that passively diffuse into the cytosol, ADCs are actively taken up by targeted cells via the endosomal and lysosomal pathway, which exposes them to high levels of various proteases that are often overexpressed in human cancers[59]. Hence, we exchanged the amino-acid ester release handle with an alanine-alanine dipeptide in linker **11**-SN38, with the expectation that **11**-SN38 forms the same carboxylic acid intermediate after protease mediated cleavage that **6**- and **10**-SN38 form upon esterase cleavage. Although such structures have not previously been explored in the context of ProTide prodrugs, they were recently described in phosphonamidite- and phosphoramidate-based fluorescent probes designed to study carboxypeptidases, representing the first report to implicate carboxypeptidases in ProTide activation[60]. **11**-SN38 exhibited similar potencies on the targeted cell lines, but reduced selectivity (targeted vs. isotype-ADC) compared to the esters **3, 8**, and **9** (Fig. 3c).

Other known release triggers exploit the reductive environment or beta-glucuronidase activity in endo-/lysosomes[49,50]. Hence, we also synthesized reductively cleavable disulfide **12** and GlcA protected alcohol **13** and explored if liberated sulfhydryl or hydroxyl groups would perform a 5-membered cyclization at the phosphorus and facilitate release of the attached drug. The selectivity of ADCs **12**-SN38 and **13**-SN38 for the targeted cell lines was comparable to the glycine derivative **8** (Fig. 3c). Even though slightly reduced, both targeted constructs showed decent activities, supporting a release mechanism that involves the liberation of a nucleophile (COOH, OH and SH) in delta position of the central P-atom which can release the attached drug by five-membered cyclization.

Another property of ADCs that is discussed to have a crucial impact on their performance is their hydrophobicity. To determine the hydrophobicity of the synthesized ADCs and how the different linkers **3** and **6**-**13** influence these, we characterized the conjugates by hydrophobic interaction chromatography (HIC). The HIC-retention time can be used as a measure for overall ADC hydrophobicity and previous reports conclude that earlier eluting, more hydrophilic ADCs have beneficial PK properties[61]. The free carboxylic acid in dialanine linker **11** comprised the most hydrophilic DAR8 SN38-ADC tested herein (Fig. 3d). From the ester series linker **6** and **7** delivered more hydrophobic ADCs, whereas the glycine derivative in linker **8** yielded a slightly more hydrophilic ADC compared to linker **3**. At the same time, an increased hydrophilicity of the ADCs was observed with the isopropyl substituent in **9** and **10** compared to all the *tert*-butyl

https://doi.org/10.1038/s41467-026-68605-y

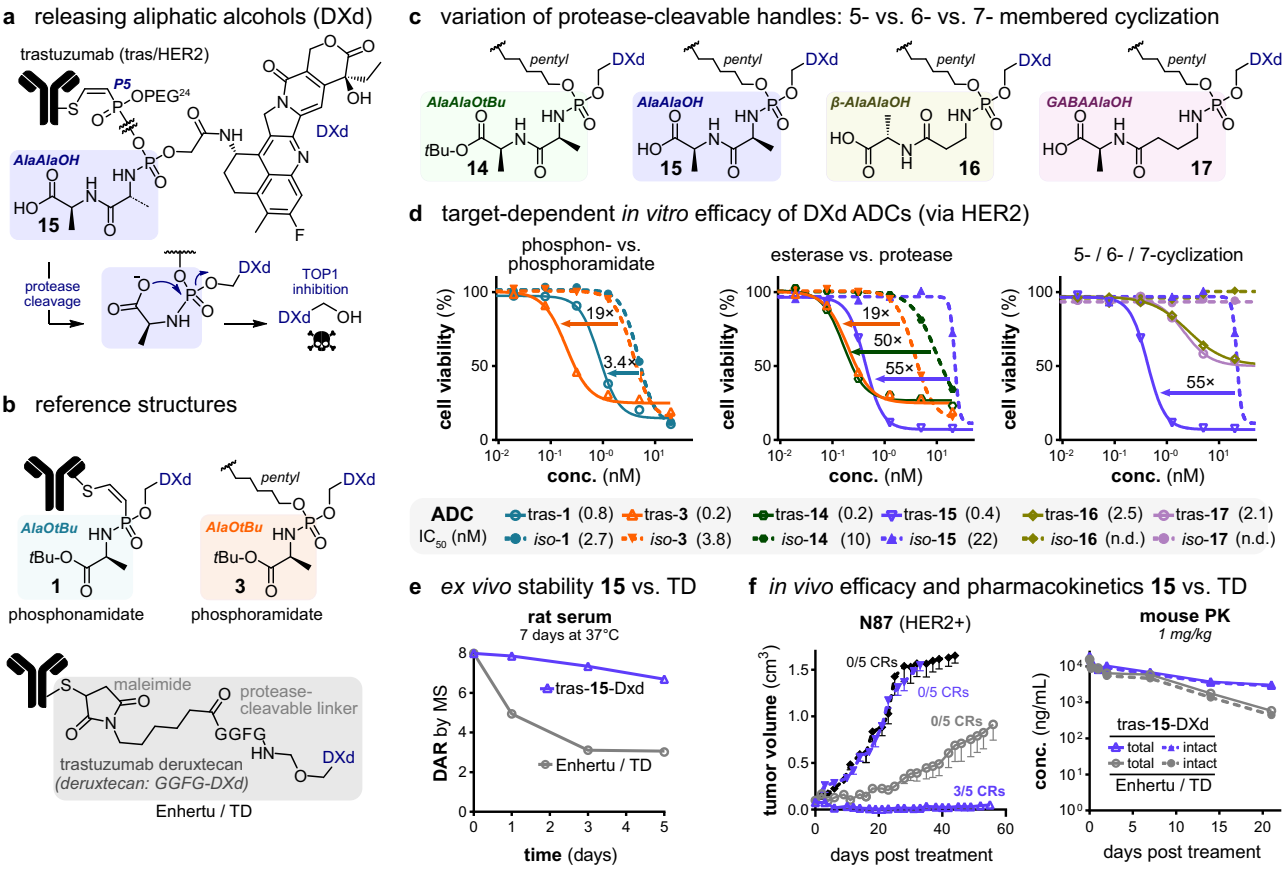

Fig. 4 | Evaluation of ADCs with phosphorus-based self-immolative linkers and aliphatic alcohols, exemplified with DXd. a DAR8 ADCs from trastuzumab (tras/anti-HER2) using DXd and protease-cleavable release handles (highlighted with purple background) that initiate release via 5-membered cyclization. **b** Linker-payload structures **1**-DXd (highlighted with turquoise background) and **3**-DXd (highlighted with orange background) after cysteine conjugation. **c** Linker-payload structures **14**–**17**-DXd after cysteine conjugation. Alanine-alanine *tert*-butyl ester release handle highlighted with green Background, di-alanine release handle highlighted with purple background, beta-alanine-alanine release handle highlighted with yellow background and gamma-aminobutyric acid-alanine release handle highlighted with red background. **d** Evaluation of trastuzumab-**1**- (turquoise) and -**3**-DXd (orange) in comparison to isotype controls. Comparison of esterase cleavable trastuzumab-**3**-DXd (orange) to protease cleavable **14**-DXd (green) and **15**-DXd (purple) in comparison to isotype controls (middle). Comparison of trastuzumab-**15**-DXd (purple), **16**-DXd (brown) and **17**-DXd (pink) that can form a 5-, 6-, or 7-membered ring after protease cleavage in comparison to isotype controls (right). Anti-proliferative dose response curves for targeting ADCs (solid) and isotype-ADCs (dashed) on SKBR-3 cells (HER2 +). Mean, $n = 2$. **e** Rat serum stability: DAR measured by mass spectrometry of tras-**15**-DXd (purple) or TD (gray) after incubation for up to 5 days in rat serum at 37 °C. Mean, $n = 2$. **f** In vivo efficacy evaluation of tras-**15**-DXd (purple open upward-pointing triangle), iso-**15**-DXd (purple filled downward-pointing triangle), TD (gray open circle) or vehicle (black filled diamond) (left). Female CB17 SCID mice have been implanted with cell-culture-derived xenograft model based on N87 cells in matrigel. Treatment started once when tumor volumes reached 0.1–0.15 cm^3. Mice were treated once at day 0 with 1 mg/kg of the ADCs. Each group consisted of $n = 5$ females each. Shown is the Mean ± SEM of the 5 animals. TD trastuzumab deruxtecan, CR complete responses of total mice treated. Pharmacokinetic analysis of CB17-SCID mice treated with 1 mg/kg of either tras-**15**-DXd (purple) or TD (gray) (right). Samples were drawn after several timepoints throughout the 3-week study period. The serum samples were analyzed by ELISA for total mAb with anti-HER2 antibodies (straight line) and intact ADC with anti-payload antibodies (dotted line).

derivatives. Of note, changing the *tert*-butyl- to the isopropyl-ester did not change the effect on normal human primary cells (Fig. S1c).

Taken together, the results summarized in Fig. 3 illustrate that stability, release efficiency and hydrophilicity of phosphoramidate-based drug-linker can be tuned by altering the substitution pattern around the phosphorous atom, covering a range from SG-like instability to a more targeted delivery of SN38. This stability tuning could be useful in the future to identify the optimal linker for a certain target that requires either stable delivery or a certain level of instability to match different levels of healthy tissue expression.

Establishment of phosphorus-based self-immolative handles for the targeted delivery of aliphatic alcohols exemplified with DXd

Next, we chose the TOP1-Inhibitor DXd as model payload, carrying a primary alcohol. DXd is the payload of the marketed ADC trastuzumab deruxtecan (TD/Enhertu)[62]. We synthetically introduced DXd into the phosphorus(V)-based linker systems **1** and **3** as already described for SN38 and conjugated the resulting linker-payloads to trastuzumab and an isotype antibody to test for targeted delivery via the HER2 antigen (Fig. 4a and b). Compared to what we observed for SN38, the phosphonamidate-based linker **1** delivered DXd into the targeted cell line with a 3-fold better selectivity compared to the isotype ADC (Fig. 4d). Like for SN38, a phosphoramidate release handle in **3**-DXd was superior to phosphonamidates in **1**-DXd (Fig. 4d), displaying a higher potency ($IC_{50} = 0.2$ nM versus 0.8 nM) and a larger selectivity (19x versus 3.4x) for the targeted cell line. Next, we exchanged the esterase cleavable handle to a protease responsive dialaninyl-cleavage site in linker **14**-DXd (Fig. 4c). In stark contrast to the protease cleavable **11**-SN38, we observed an improved linker stability that resulted in a more selective (50×) delivery of the payload. We assign this enhanced stability to decreased leaving group properties (=higher pKa) of the aliphatic hydroxyl group in DXd. The selectivity of **14**-DXd

https://doi.org/10.1038/s41467-026-68605-y

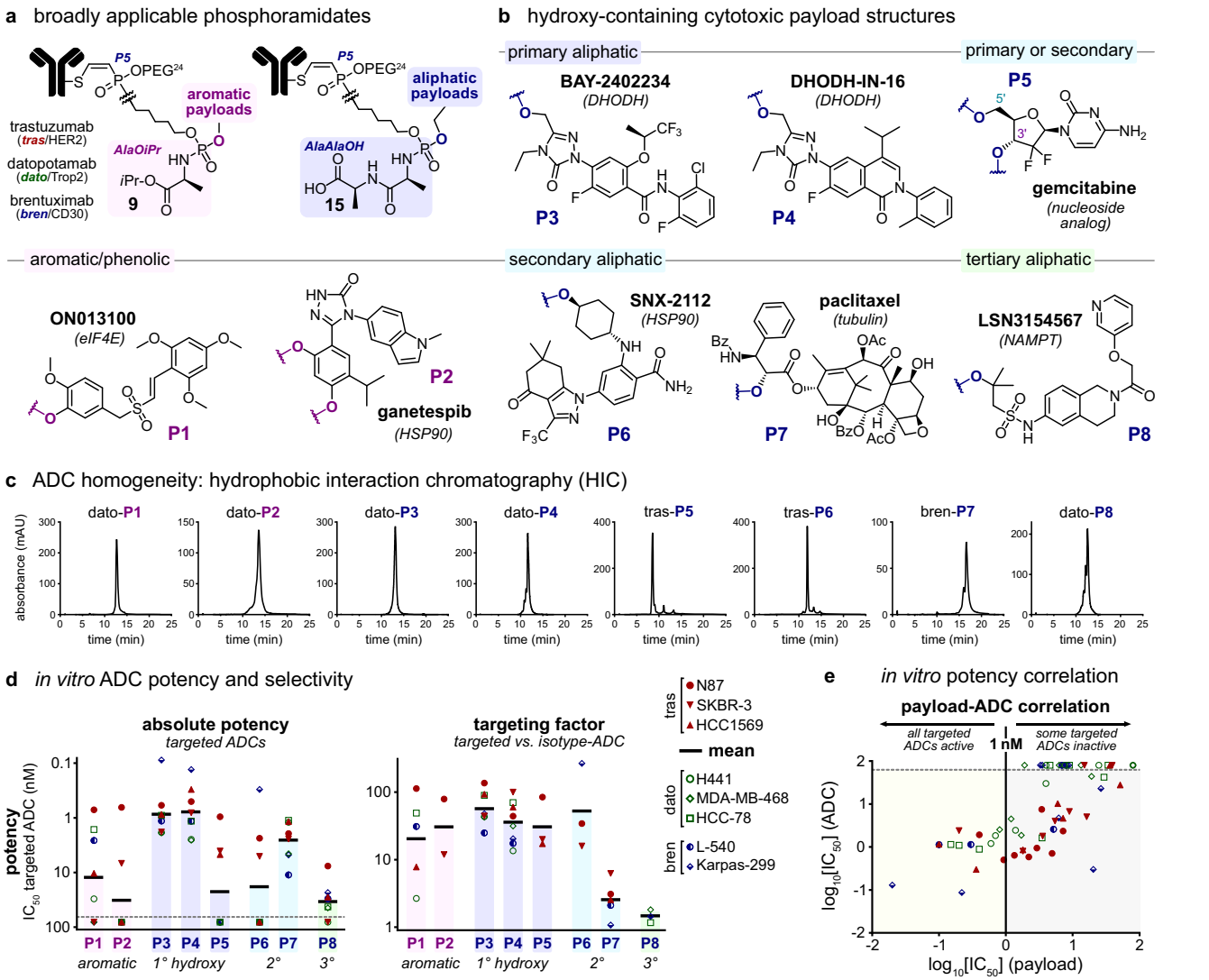

Fig. 5 | Combination of the phosphoramidate-based linker systems with structurally diverse hydroxy-containing cytotoxins exhibiting diverse MOAs. **a** DAR8 ADCs from trastuzumab (tras/anti-HER2, red), datopotamab (Dato/anti-Trop2, green) or brentuximab (bren/anti-CD30, blue) in combination with linker **9** for aromatic (highlighted with pink background) and linker **15** for aliphatic payloads (highlighted with purple background). **b** Ganetespib and ON01300 have been conjugated via linker **9**; BAY-2402234, DHODH-IN-16, SNX2112, paclitaxel and LSN3154567 have been conjugated via linker **15**. Pink shading refers to aromatic payloads, purple shading refers to primary aliphatic payloads, blue shading refers to secondary aliphatic payloads and green shading refers to tertiary aliphatic payloads. **c** HIC chromatograms to analyze ADC homogeneity from every payload. A DAR of 8 has been confirmed by MS. **d** Potency and selectivity of the different ADCs for the targeted cell line. Tras-ADCs were tested on N87 (red solid circle), SKBR-3 (red solid downward-pointing triangle) and HCC1569 (red solid upward-pointing triangle) (HER2 +), bren-ADCs were tested on L-540 (blue half-filled circles) and Karpas-299 cells (blue half-filled diamonds) (CD30 +), dato-ADCs were tested on H441 (green open circles), MDA-MB-468 (green open diamonds) and HCC-78-cells (green open squares) (Trop2 +), while the bren conjugates served as isotypes for the HER2+ and Trop2 + -cell lines and vice versa. The ADC selectivity is plotted as the ratio of IC_{50} isotype-/IC_{50} targeted ADC. The absolute potencies of the ADCs are plotted for their target-positive cell lines. Pink columns refer to aromatic payloads, purple columns refer to primary aliphatic payloads, blue columns refer to secondary aliphatic payloads and green columns refer to tertiary aliphatic payloads. The black bars show the mean values for the eight cell lines (targeted via three distinct receptor-antibody-pairs) and serve as orientation to compare the different payloads. **e** Correlation between the proliferation inhibition IC_{50} of unconjugated payloads (x-axis) over the ADCs on the same cell line (y-axis) (N87, red solid circle; SKBR-3 red solid downward-pointing triangle; HCC1569, red solid upward-pointing triangle; L-540, blue half-filled circles; Karpas-299, blue half-filled diamonds; (CD30 +); H441, green open circles; MDA-MB-468, green open diamonds; HCC-78-cells, green open squares). ADCs above the dotted line were inactive at the highest tested concentration of 80 nM and excluded from the correlation. Dose-response curves for ADCs and payloads are shown in Fig. S8.

was even more increased using linker **15** (55×) that possesses a terminal carboxy group instead of the tert-butyl ester as shown in Fig. 5c. The terminal carboxy group is also desired, since it adds additional hydrophilicity to the linker system, as shown for SN38 in Fig. 3d.

To better understand whether Dxd release involves an attack of the alanine carboxy group on the central phosphorus via a 5-membered intermediate, we synthesized linker **16**- and **17**-DXd, requiring formation of less favored 6- or 7-membered rings for a similar drug release after protease cleavage. ADCs of both linkers were almost inactive on the targeted cell lines (Fig. 4d), underlining the mechanism that is shown in Fig. 1b, requiring a 5-membered-cyclization from a free carboxylate to the central phosphorus atom for efficient release. Comparing the high efficiency of linker **15** with the inactive **16** and **17** further allows the conclusion that release of non-derivatized DXd-OH is required to exhibit in vitro potency and that linker **15** is the most suited for delivery of aliphatic alcohols.

Next, we compared **15**-Dxd head-to-head with the state-of-the-art protease-cleavable linker-payload GGFG-DXd in a set of in vitro and

in vivo experiments. In Fig. 4e, we assessed ADC-stability in rat serum and demonstrated increased stability of tras-**15**-DXd compared to TD. It should be noted that the serum stability of **15**-DXd is even higher than that of linker **3**-SN38 (Fig. 2f). We attribute this to the higher pKa of the aliphatic alcohol in DXd making it a worse leaving group compared to the aromatic alcohol in SN38, leading to less drug hydrolysis in serum. We confirmed target selectivity for tras-**15**-DXd and TD in vitro on a larger panel of cell lines without activity on non-targeted cell lines (Fig. S4). Finally, we showed that tras-**15**-DXd effectively eradicates HER2+ tumors in vivo, whereas an iso-**15**-DXd did not show any anti-tumor effect (Fig. 4f). Only the linker system described herein showed complete responses in three out of five animals at a dose of 1 mg/kg, whereas no complete responses were observed for the group that has been treated with TD at the same dose. Pharmacokinetic analyses by ELISA of blood samples drawn from this study revealed an excellent PK profile with slow clearance of tras-**15**-DXd and superimposable assay results for total antibody and intact ADC, highlighting outstanding linker stability. In contrast, TD was more rapidly cleared from circulation (Fig. 4f). This might be attributed to increased hydrophilicity of tras-**15**-DXd in comparison to TD, as evidenced by HIC retention time (Fig. S4c). Increased ADC hydrophilicity has been previously shown to lower ADC clearance in vivo[18]. Collectively, these results underline that the phosphoramidate linker systems described herein enable an efficient and selective delivery of DXd into the targeted cell with a superior in vivo efficacy compared to an approved ADC based on the same antibody and payload.

Application of phosphoramidate linkers to the antibody-mediated delivery of structurally diverse hydroxy-containing cytotoxins exhibiting diverse MOAs

Finally, with the overall goal to identify novel ADC payloads, we aimed to apply our linker systems to a wider range of hydroxy-containing antiproliferative agents. For all drugs with aromatic alcohols, we employed linker **9** and for all drugs with aliphatic alcohols linker **15**, both identified as optimal linker in terms of potency, selectivity and ADC hydrophilicity. To confirm the suitability of these two linker systems we again investigated both intracellular cleavability and extracellular stability in circulation. In addition to the esterase cleavage experiments on isolated linker payloads **3, 9** and **10**-SN38, we also demonstrated that other proteases such as cathepsin A (CatA) are able to release the payload from **3**-SN38, **9**-SN38, but importantly also from **15**-DXd. Figure S5 This data suggests that both, the esterase cleavage handle in linker **9** and the protease cleavage handle in linker **15** can be cleaved by multiple enzymes in the endosomal-lysosomal system, similar as previously described for more traditional linker systems[63]. We believe that the systems described herein achieve cancer specificity by the targeting antibody rather than a tumor- selective release of the attached drug. To further assess the extracellular linker stability, we submitted the isolated linker-payloads **9**-SN38 and **15**-DXd to a neutrophile elastase assay (Fig. S6a–c). Susceptibility to neutrophile elastase cleavage has been identified as a potential cause of premature drug release leading to neutropenia[64]. Interestingly, both linker systems behaved differently, showing drug release only from the esterase cleavable **9**-SN38, while **15**-DXd showed no signs of DXd release in the presence of human neutrophile elastase. To study this further, we also tested the ADCs from **9**-SN38 and **15**-DXd revealing only minor or no signs of enzymatic linker cleavage, respectively, while a control ADC utilizing mc-VC-PAB-MMAE as linker-payload underwent extensive degradation, releasing 90% of the expected NH_2-Citrulline-PAB-MMAE fragment over 24 hours as previously reported (Fig. S6d)[64]. This data suggests that the protease cleavable linker **15** is fully stable, while there is a potential liability for the esterase based system **9** towards neutrophile elastase. However, in the much more relevant ADC format, we were able to demonstrate that the severeness of this instability is significantly lower compared to approved Vedotin-based ADCs such as Adcetris. This could be confirmed also in human serum stability assays of ADCs from **9** and **15** (Fig. S6e).

Next, we employed the HSP90 inhibitor ganetespib[65] and the elongation factor inhibitor ON013100[66] as examples for aromatic payloads; the nucleoside analogue gemcitabine[67] and the dihydroorotate dehydrogenase (DHODH) inhibitors BAY-2402234[68] and DHODH-IN-16[69], as primary alcohols; the HSP90 inhibitor SNX2112[70] and the tubulin inhibitor paclitaxel[71] as secondary alcohols and the nicotinamid phosphoribosyltransferase (NAMPT) inhibitor (LSN3154567)[72] as example for a tertiary alcohol (Fig. 5b). All linker-drugs were conjugated to the three different antibodies trastuzumab (HER2-targeting), datopotamab (Trop2-targeting) and brentuximab (CD30-targeting) (Fig. 5a). Even though all these drugs differ in hydrophobicity and more hydrophobic payloads lead to ADCs with a higher HIC retention time, it was still possible to generate homogenous DAR8 constructs from the inhibitors described herein (Fig. 5c and Fig. S7). Next, to investigate the applicability of those payloads, the ADCs were tested in eight different cell lines. Trastuzumab-based ADCs were investigated in cell killing assays on the HER2-positive solid cancer cell lines N87, SKBR-3 and HCC1569; datopotamab-based ADCs on the Trop2-positive solid cancer cell lines H441, HCC-78, and MDA-MB-468, and brentuximab-based ADCs on the CD30-positive lymphoma cancer cell lines L-540 and Karpas-299 (Fig. S8). This in vitro evaluation revealed successful target-dependent delivery of all chosen payloads as can be seen by the IC50 values and selectivity factors in Fig. 5d. This is highly remarkable, since it firstly confirms broad applicability to very different chemical hydroxyl groups and secondly shows the ability to unlock novel payloads using phosphoramidate based self-immolative handles. Even though single examples of ADCs carrying HSP90-[73], NAMPT-inhibitors[72] and paclitaxel[74] have been described in the literature, this is the first time that ADCs carrying nucleoside analogues, DHODH- or an elongation factor-inhibitors are described and documented with in vitro potency[7]. Potency generally ranged between IC_{50} values of 0.1 nM and 60 nM. Whereas most of the payloads showed a beneficial ratio between targeted and non-targeted ADCs with a targeting factor of 10, paclitaxel and LSN315456 demonstrated only modest selectivity for the targeted cell line (Fig. 5d). It should be noted that universal linker **9** and **15** for aromatic or aliphatic alcohols were used in this screen and that stability tuning by phosphoramidate modifications, as reported for SN38, might further optimize the stability and release for each payload described here.

To better understand the potency differences of the different payloads across cell lines, we plotted the antiproliferative activity of all the unconjugated payloads against the effectiveness of the targeted ADCs (Fig. 5e). As expected, the more effective an antiproliferative drug is in its unconjugated form on a certain cell line, the more active is also its respective ADC. Remarkably, all payloads with activity below 1 nM also showed activity when delivered by an ADC, clearly demonstrating the broad applicability of the described linker system to efficiently deliver chemically diverse hydroxyl groups. Payloads with a lower activity than 1 nM led to active ADCs in some cases but were more likely to be inactive. The observation that subnanomolar potency of a cytotoxin is a requirement for an ADC payload is in line with previous predictions[4,75]. However, to the best of our knowledge, this is the first time that this has been investigated more systematically in one comparable experiment with a broad range of different drugs conjugated via the same linker system.

Finally, we chose gemcitabine as a showcase payload to further highlight the potential of the phosphoramidate-based linker system described herein to unlock unusual and scarcely described payloads for targeted drug delivery with ADCs. Gemcitabine attracted our interest as potential ADC-payload since it is a clinically-established chemotherapeutic with a known safety profile but significant limitations in rapid clearance from the body, requiring high gram doses over time[76]. Antibody-mediated drug delivery could overcome those

https://doi.org/10.1038/s41467-026-68605-y

pharmacokinetic limitations, unlocking gemcitabines' full therapeutic potential. ADCs with both regioisomers of **15**-gemcitabine, connected via the primary 5′-hydroxy or the secondary 3′-hydroxy, were synthesized from trastuzumab (Fig. 6a) and evaluated for target-mediated antiproliferative activity in vitro. Confirming the broad applicability of the linker systems described herein, ADCs attached via the primary or secondary alcohol of gemcitabine proved to be equally active on the targeted cell line (Fig. 6b). As depicted in Fig. 6a, gemcitabine requires 5′-phosphorylation via deoxycytidine kinase followed by pyrophosphorylation to exhibit its cytotoxic activity. Co-incubation of ADC-treated cells with DI-87, an inhibitor for the initial phosphorylation, depleted activity for both ADCs to the level of unmodified trastuzumab only. Thus, we conclude that the ADCs tracelessly release gemcitabine and not any related phosphorylated species originating from the phosphoramidate linker system described herein.

Finally, tras-**15**-5′-gemcitabine was evaluated in vivo in the N87 tumor model. Encouragingly, we observed a strong anti-tumor effect after a single dose of 20 mg/kg (Fig. 6c). This effect proved to be selective, since the isotype ADC was completely inactive at the same dose. In parallel, the anti-tumor effect of trastuzumab (20 mg/kg) and unconjugated gemcitabine, dosed at 0.28 mg/kg corresponding to the dose administered in the DAR8 ADC format, was only slightly higher than for the vehicle control. This effect most likely reflects the tumor growth inhibition of trastuzumab alone, already observed in vitro (Fig. 6b), while unconjugated gemcitabine can be considered inactive at this low dose due to rapid clearance from circulation, as previously reported. Considering that the dose of gemcitabine administered in the ADC format is almost 1000-times lower than that typically administered over multiple injections to achieve tumor regression[77], the in vivo effect observed here is particularly remarkable. We attribute this enhanced activity to improved pharmacokinetics. In fact, clearance of the DAR8 tras-**15**-5′-gemcitabine is highly similar to unconjugated trastuzumab, as shown in Fig. 6c. Hence, the linker system described here widens the therapeutic window for gemcitabine by stably delivering the active payload to the tumor over a long period of time after single administration, whereas unconjugated gemcitabine is rapidly metabolized and excreted in vivo[78]. Tras-**15**-5′-gemcitabine has also been evaluated for toxicity in rats in doses up to 150 mg/kg (Fig. S9). Not a single sign of toxicity was observed at the highest dose tested, which is 7.5 times higher than the effective dose used in the in vivo efficacy experiment, clearly pointing towards large therapeutic indices that can be reached with the linker systems described herein.

To conclude, we identified phosphoramidates, substituted with a release handle at the nitrogen atom, a linker for antibody modification and the to-be-delivered drug at the oxygen substituents as broadly applicable functional motifs for the delivery of aromatic- as well as primary-, secondary- and tertiary-alcohol-containing payloads. The stability and release of the payload can be tuned via simple modifications of the phosphoramidate substituents, allowing adaptation to various alcohols of different pKa or matching the linkage stability to the requirements of the antibodies' target. Moreover, as long as the trigger releases a nucleophile that can form a five-membered ring with the central phosphorus atom, the release can be initiated via various intracellular stimuli including esterases, proteases and glucuronidase, as well as reductive conditions. While several functional groups have been previously used to conjugate hydroxy-containing payloads to antibodies, a broadly applicable solution for stable attachment in circulation and traceless release intracellularly is still unprecedented. Here, we introduce cleavable phosphoramidates as a self-immolative entity that can be broadly applied to alcohols of very different kinds (primary, secondary, tertiary and phenolic) with different electronic properties. The linker system outperformed the ones of the approved ADCs SG and TD in delivery of the respective hydroxy-containing TOP1-Inhibitors SN38 and DXd. Here, phosphoramidate-based linkers were superior in serum stability, in vivo efficacy and PK. More importantly, the simple drug-linker synthesis and conjugation of highly loaded homogenous DAR8 ADCs enabled us to repurpose and screen existing small molecule cytotoxins with various MOAs as novel ADC payloads. Highly efficacious ADCs with IC_{50} values in the nanomolar to sub-nanomolar range were synthesized. Many of those cytotoxins and MOAs were without literature precedence in drug

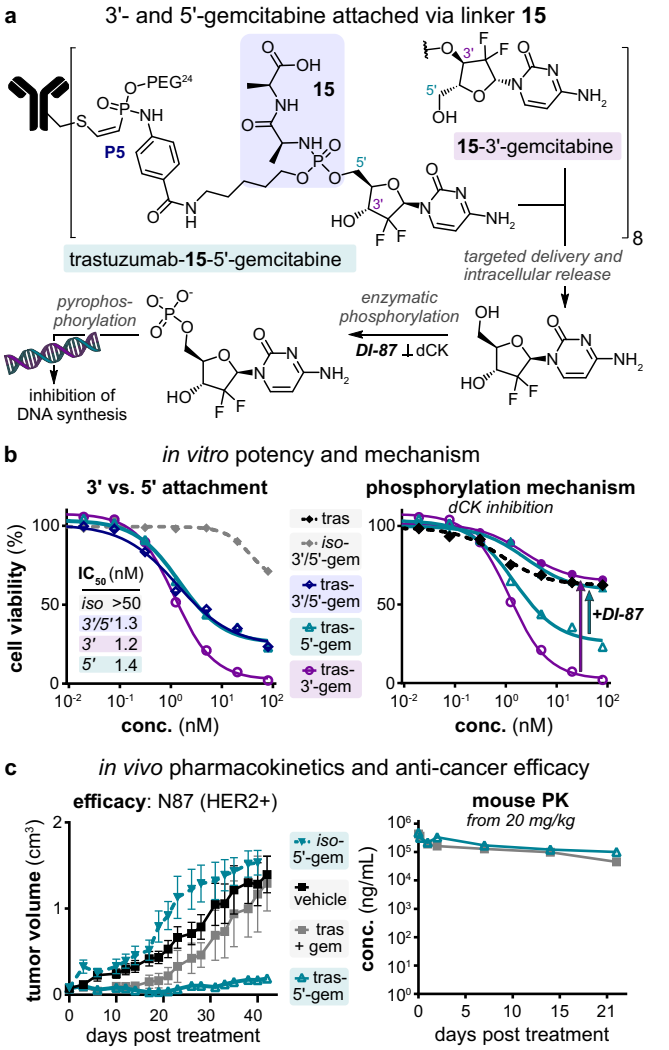

Fig. 6 | Evaluation of gemcitabine ADCs attached via linker 15 with its' primary 5′ or its secondary 3′ hydroxyl groups. a Structure of the two different ADCs and schematic representation of the intracellular MOA. Di-alanine release handle is highlighted with purple background, 3′-O-modified Gemcitabine is highlighted with pink shading and 5′-O-modified gemcitabine is highlighted with turquoise shading. **b** In vitro evaluation of trastuzumab-gemcitabine (tras/anti-HER2) ADCs attached via 5′- (turquoise), 3′- (pink) or a mixture of 5′/3′-hydroxyl (purple) on N87-cells in comparison to isotype control (gray) (left) and inhibition of antiproliferative activity via DI-87 (right). Anti-proliferative dose response curves for targeting ADCs (solid) and isotype-ADCs (dashed) on SKBR-3 cells (HER2 +). Mean, $n = 2$. **c** In vivo PK and efficacy evaluation of tras-**15**-gemcitabine. In vivo efficacy was evaluated in female CB17 SCID mice have been implanted with cell-culture-derived xenograft model based on N87 cells in matrigel. Treatment started once tumor volumes reached 0.1–0.15 cm^3 with 20 mg/kg on day 0 of either tras-**15**-5′-gemcitabine (turquoise open upward-pointing triangle), iso–**15**-5′-gemcitabine (turquoise filled downward-pointing triangle) or 20 mg/kg tras + 0.28 mg/kg unconjugated gemcitabine (gray filled squares) or vehicle (black filled squares). Each group consisted of $n = 5$ females each. Shown is mean ± SEM of the 5 animals. PK has been evaluated in CB17-SCID mice treated with 20 mg/kg at $T = 0$ of trastuzumab only (gray) or tras-**15**-5′-gemcitabine (turquoise). Samples were drawn after several timepoints throughout the 3-week study period and analyzed by ELISA for total mAb.

delivery. The broad dataset with ten cytotoxins conjugated to a variety of antibodies allowed us to support the general hypothesis in targeted drug delivery that sub-nanomolar potency of a small molecule cytotoxin is needed to generate effective ADCs. Payloads with lower potency on a certain cell line on the other hand can completely lack activity in vitro. Finally, for the first time, we demonstrate in vivo efficacy of an ADC based on gemcitabine. The antibody-like PK profile of this DAR8 ADC, enabled by the phosphoramidate linker system, leads to in vivo activity at doses 1000 times lower than those typically administered for unconjugated gemcitabine. We are convinced that the broad compatibility of the linker system described herein with structurally diverse alcohols, combined with the efficient production of homogenous DAR8 ADCs from readily available pharmacologically active small molecules will allow for faster identification of suitable payloads to expand the currently limited panel of only three MOAs in approved ADCs. This will broaden the scope of ADC modalities with great potential in addressing drug resistance mechanisms in patients.

Methods

General method for the conjugation of linker payloads

50 µl of the antibody solution of 10.0 mg/ml in P5-conjugation buffer (50 mM Tris, 1 mM EDTA, 100 mM NaCl, pH 8.3 at RT) were mixed with 3.33 µl of a 10 mM TCEP solution in P5-conjugation buffer. Directly afterwards, 1.67 µl of a 40 mM solution of the linker-payload constructs dissolved in DMSO were added. The mixture was shaken at 350 rpm and 25 °C for 16 h. The reaction mixtures were purified by preparative size-exclusion chromatography with a 25 ml Superdex™ 200 Increase 10/300GL (Cytiva, Sweden) and a flow of 0.8 ml/min eluting with sterile PBS (Merck, Germany). The antibody containing fractions were pooled and concentrated by spin-filtration (Amicon® Ultra- 2 mL MWCO: 30 kDa, Merck, Germany).

In vitro cytotoxicity on cancer cells

To investigate the cytotoxicity of ADCs and unconjugated cytotoxins, 5000 cells per well were incubated for 7 days or 4 days, respectively, with increasing concentrations of the ADCs (0.18–12,000 ng/ml = 0.0012–80 nM) or small molecules (0.015–1000 nM) to generate a dose–response curve. Before the analysis of cell viability, the spent medium containing dead cells was removed and fresh medium was added. Killing was analyzed using resazurin cell viability dye at a final concentration of 55 µmol/L (Merck) by dividing the fluorescence from control cells in medium by the fluorescence of ADC-treated cells. Fluorescence emission at 590 nm was measured on a microplate reader Infinite 200 PRO (Tecan Group Ltd.).

In vitro bystander activity

For the supernatant-based bystander experiment, 20,000 Trop2-positive MDA-MB-468 cells were seeded in 100 µl medium and treated with saci-**3**-SN38 at concentrations ranging from 0.18 to 12,000 ng/ml. After 5 days, 50 µl of the supernatant of the treated cells was transferred to 50 µl of Trop-negative SW-620 (5000 cells/well) and incubated for 5 days. Resazurin readout was performed as described for the in vitro toxicity evaluation.

Cell lines

Cell lines were purchased from the "German Collection of Microorganisms and Cell Cultures" (DSMZ, Leibniz Institute, Germany), American Type Culture Collection (ATCC, USA), Japanese Collection of Research Bioresources (JCRB) via Tebubio (France), Merck (Germany) or Thermo Fisher Scientific (USA): SR-786 (ACC 369, DSMZ; RRID:CVCL_1711; sex: male), L-540 (ACC 72, DSMZ; RRID:CVCL_1362; sex: female), Karpas-299 (Merck, RRID:CVCL_1324); sex: male), NCI-N87 (CRL-5822, ATCC; RRID:CVCL_1603; sex: male), SK-BR-3 (ACC 736, DSMZ; RRID:CVCL_0033; sex: female), HCC-1569 (CRL-2330, ATCC; RRID:CVCL_1255; sex: female), H441 (HTB-174, ATCC; RRID:CVCL_1561; sex: male), MDA-MB-468 (ACC 738, DSMZ; RRID:CVCL_0419; sex: female), HCC78 (ACC 563, DSMZ; RRID:CVCL_2061; sex: male), SW620 (300466, Tebubio; RRID:CVCL_0547; sex: male), ExpiCHO-S (A29127, Thermo Fisher Scientific; RRID:CVCL_5J31; sex: female). Cells were cultured according to the manufacturer's instructions in either RPMI 1640 or DMEM medium supplemented with GlutaMAX (Gibco, Thermo Fisher Scientific, USA) and 10–20% fetal bovine serum (FBS; Gibco, Thermo Fisher Scientific, USA). Cell lines for antigen or antibody production were cultivated in their proprietary medium (Thermo Fisher Scientific, USA). For passage or for assay setup, the adherent cells were detached by TrypLE Express Enzyme (Thermo Fisher Scientific, USA) according to manufacturer's instructions and splitted or seeded accordingly.

A mycoplasma test is performed using MycoAlert® Mycoplasma Detection Kit (Lonza, Switzerland) according to the manufacturer's instructions every 6 month (latest test: 04/2025). Cell line authentication was performed at the cell bank and is conducted internally every 6 months via SNP typing (latest test: 04/2025). Cell lines are used at a maximum passage of 30 and then re-thawed for further experiments.

In vivo efficacy

All animal experiments were conducted in accordance with German animal welfare law and approved by local authorities. Mice were housed at room temperature (24 ± 2 °C) with a relative humidity of 50 ± 10% at artificial light with a 12 h dark and 12 h light rhythm. Mice were 8 weeks old at the start of the studies.

For the SN38 study, 1×10^7 MDA-MB-468 cells (50 µl + 50 µl Matrigel) were subcutaneously injected to female CB-17/Icr-Prkdcscid/scid/Rj mice. Treatment was initiated when tumors reached a tumor volume of about 0.1 cm^3 9 days after implantation. 5 animals per group were treated twice at day 9 and day 13 with 10 mg/kg each treatment day of either saci-**3**-SN38, iso-**3**-SN38 or Trodelvy and compared to a vehicle treated group.

For the DXd study, 2×10^6 N87 cells were subcutaneously injected to female CB-17/Icr-Prkdcscid/scid/Rj mice. Treatment was initiated when tumors reached a tumor volume of about 0.1 cm^3 7 days after implantation. 5 animals per group were treated at day 7 with 1 mg/kg of either tras-**15**-DXd, iso-**15**-DXd or Enhertu and compared to a vehicle treated group. For PK analysis, blood samples were drawn from one mouse per group of the tras-**15**-DXd and the Enhertu group after 5 min, 4 h, 1 day, 2 days, 7 days, 14 days and 21 days and analyzed for ADC exposure by ELISA as described below.

For the gemcitabine study, 2×10^6 N87 cells were subcutaneously injected to female CB-17/Icr-Prkdcscid/scid/Rj mice. Treatment was initiated when tumors reached a tumor volume of about 0.1 cm^3 4 days after implantation. 5 animals per group were treated at day 4 with either 20 mg/kg of tras-**15**-gemcitabine, 20 mg/kg of iso-**15**-gemcitabine or 20 mg/kg tras and 0.28 mg/kg gemcitabine and compared to a vehicle treated group. For PK analysis, blood samples were drawn from one mouse per group of the tras-**15**-gemcitabine and the tras + gemcitabine group after 5 min, 4 h, 1 day, 2 days, 7 days, 14 days and 21 days and analyzed for ADC exposure by ELISA as described below. Mice were treated via intravenous injection after randomization into treatment and control groups. Tumor volumes, body weights and general health conditions were recorded throughout the whole study.

In vivo toxicity

All animal experiments were conducted in accordance with Hungarian animal welfare law and approved by local authorities. Sprague-Dawley rats (Charles River Laboratories) were housed at room temperature (22 ± 3 °C) with a relative humidity of 30–70% at artificial light with a 12 h dark and 12 hours light rhythm. 7-week-old male rats were treated once at day 0 with either 50, 100 or 150 mg/kg tras-**15**-gemcitabine. The animals were observed for 22 days. Bodyweight and food-

consumption was monitored throughout the study. Blood samples for the PK analysis were drawn after 1 h, 7 days, 14 days and 21 days. The samples were analyzed for ADC exposure as described below. Heamatology and clinical chemistry was measured 5 days before dosing and 7 days, 14 days and 21 days after dosing.

Analysis of the in vivo samples by ELISA to assess the pharmacokinetic of the ADCs

To evaluate the PK of the ADCs in vivo, the total antibody concentration was measured at different time points in serum of ADC-treated mice or rats from the in vivo studies described above. Total trastuzumab- and derived ADC levels were analyzed in mouse- and rat serum serum over the range 2000–15.6 ng/mL. Clear Nunc flat bottom MaxiSorp 96-well plate (Thermo Fisher Scientific, USA) was coated with recombinant human HER2 antigen diluted in DPBS (Thermo Fisher Scientific, USA) to a final concentration of 1 μg/mL and incubated over night at 4 °C. Excess antigen was removed by washing with PBST (DPBS + 0.05% Tween 20, Merck, Germany) and plates were blocked for 1 h at room temperature in blocking solution (2 % albumin in PBST; Merck, Germany). Prepared standards (2000–15.6 ng/ml) of the respective ADCs, QCs and serum test samples were incubated at room temperature for 1 h. Samples were detected using HRP-conjugated goat anti-human kappa light chain secondary antibody (Thermo Fisher Scientific, USA, Cat# A18853, RRID:AB_2535630) at a 1:12,000 dilution (final concentration 0.083 μg/mL) for 1 h at room temperature. Antibodies were detected using Ultra-TMB substrate (Thermo Fisher Scientific, USA) for 10 min at room temperature followed by stopping the reaction with 1 M sulfuric acid (Merck, Germany). The absorbance at a wavelength of 450 nm was measured on an Infinite 200 Pro plate reader (Tecan, USA).

Reporting summary

Further information on research design is available in the Nature Portfolio Reporting Summary linked to this article.

Data availability

The authors declare that the data supporting the findings of this study are available within the paper and its Supplementary Information files. Should any raw data files be needed in another format they are available from the corresponding author upon request. Source data are provided with this paper.

References

1. Srinivasarao, M. & Low, P. S. Ligand-targeted drug delivery. *Chem. Rev.* **117**, 12133–12164 (2017).
2. Dumontet, C., Reichert, J. M., Senter, P. D., Lambert, J. M. & Beck, A. Antibody–drug conjugates come of age in oncology. *Nat. Rev. Drug Discov.* **22**, 641–661 (2023).
3. Tsuchikama, K., Anami, Y., Ha, S. Y. Y. & Yamazaki, C. M. Exploring the next generation of antibody–drug conjugates. *Nat. Rev. Clin. Oncol.* **21**, 203–223 (2024).
4. Fu, Z., Li, S., Han, S., Shi, C. & Zhang, Y. Antibody drug conjugate: the "biological missile" for targeted cancer therapy. *Signal. Transduct. Target. Ther.* **7**, 93 (2022).
5. Fuentes-Antrás, J., Genta, S., Vijenthira, A. & Siu, L. L. Antibody–drug conjugates: in search of partners of choice. *Trends Cancer* **9**, 339–354 (2023).
6. Colombo, R. & Rich, J. R. The therapeutic window of antibody drug conjugates: a dogma in need of revision. *Cancer Cell* **40**, 1255–1263 (2022).
7. Conilh, L., Sadilkova, L., Viricel, W. & Dumontet, C. Payload diversification: a key step in the development of antibody–drug conjugates. *J. Hematol. Oncol.* **16**, 3 (2023).
8. Lyon, R. P. et al. Self-hydrolyzing maleimides improve the stability and pharmacological properties of antibody-drug conjugates. *Nat. Biotechnol.* **32**, 1059–1062 (2014).
9. Burke, P. J. et al. Optimization of a PEGylated glucuronide-monomethylauristatin E linker for antibody–drug conjugates. *Mol. Cancer Ther.* **16**, 116–123 (2017).
10. Simmons, J. K., Burke, P. J., Cochran, J. H., Pittman, P. G. & Lyon, R. P. Reducing the antigen-independent toxicity of antibody-drug conjugates by minimizing their non-specific clearance through PEGylation. *Toxicol. Appl. Pharmacol.* **392**, 114932 (2020).
11. McKertish, C. M. & Kayser, V. Advances and limitations of antibody drug conjugates for cancer. *Biomedicines* **9**. https://doi.org/10.3390/biomedicines9080872 (2021).
12. Schmitt, S. et al. Design and evaluation of phosphonamidate-linked exatecan constructs for highly loaded, stable, and efficacious antibody–drug conjugates. *Mol. Cancer Ther.* **23**, 199–211 (2024).
13. Kovtun, Y. V. et al. Antibody-drug conjugates designed to eradicate tumors with homogeneous and heterogeneous expression of the target antigen. *Cancer Res.* **66**, 3214–3221 (2006).
14. Ogitani, Y., Hagihara, K., Oitate, M., Naito, H. & Agatsuma, T. Bystander killing effect of DS-8201a, a novel anti-human epidermal growth factor receptor 2 antibody–drug conjugate, in tumors with human epidermal growth factor receptor 2 heterogeneity. *Cancer Sci.* **107**, 1039–1046 (2016).
15. Gavriel, A. G., Sambrook, M. R., Russell, A. T. & Hayes, W. Recent advances in self-immolative linkers and their applications in polymeric reporting systems. *Polym. Chem.* **13**, 3188–3269 (2022).
16. Jackson, C. P. et al. Evaluation of an ester-linked immunosuppressive payload: a case study in understanding the stability and cleavability of ester-containing ADC linkers. *Bioorg. Med. Chem. Lett.* **75**, 128953 (2022).
17. Dubowchik, G. M. et al. Cathepsin B-Labile dipeptide linkers for lysosomal release of doxorubicin from internalizing immunoconjugates: model studies of enzymatic drug release and antigen-specific in vitro anticancer activity. *Bioconjugate Chem.* **13**, 855–869 (2002).
18. Lyon, R. P. et al. Reducing hydrophobicity of homogeneous antibody-drug conjugates improves pharmacokinetics and therapeutic index. *Nat. Biotechnol.* **33**, 733–735 (2015).
19. Bargh, J. D., Isidro-Llobet, A., Parker, J. S. & Spring, D. R. Cleavable linkers in antibody-drug conjugates. *Chem. Soc. Rev.* **48**, 4361–4374 (2019).
20. Felber, J. G. et al. Cyclic dichalcogenides extend the reach of bioreductive prodrugs to harness thiol/disulfide oxidoreductases: applications to seco-duocarmycins targeting the thioredoxin system. *ACS Cent. Sci.* **9**, 763–776 (2023).
21. Bargh, J. D. et al. Sulfatase-cleavable linkers for antibody-drug conjugates. *Chem. Sci.* **11**, 2375–2380 (2020).
22. Watanabe, T. et al. Exo-cleavable linkers: enhanced stability and therapeutic efficacy in antibody–drug conjugates. *J. Med. Chem.* **67**, 18124–18138 (2024).
23. Chuprakov, S. et al. Tandem-cleavage linkers improve the in vivo stability and tolerability of antibody–drug conjugates. *Bioconjugate Chem.* **32**, 746–754 (2021).
24. Anami, Y. et al. Glutamic acid–valine–citrulline linkers ensure stability and efficacy of antibody–drug conjugates in mice. *Nat. Commun.* **9**, 2512 (2018).
25. Conilh, L. et al. Exatecan antibody drug conjugates based on a hydrophilic polysarcosine drug-linker platform. *Pharmaceuticals* **14**. https://doi.org/10.3390/ph14030247 (2021).
26. Doronina, S. O. et al. Development of potent monoclonal antibody auristatin conjugates for cancer therapy. *Nat. Biotechnol.* **21**, 778–784 (2003).

27. Staben, L. R. et al. Targeted drug delivery through the traceless release of tertiary and heteroaryl amines from antibody–drug conjugates. *Nat. Chem.* **8**, 1112–1119 (2016).
28. Wharton, T., Crawshay-Williams, F., Schober, T., Floto, R. A. & Spring, D. R. Unlocking amides: a general method for the self-immolative release of amide-containing molecules. *Angew. Chem. Int. Ed.* **63**, e202402267 (2024).
29. Dunsmore, L. et al. Controlled masking and targeted release of redox-cycling ortho-quinones via a C–C bond-cleaving 1,6-elimination. *Nat. Chem.* **14**, 754–765 (2022).
30. Kolakowski, R. V. et al. The methylene alkoxy carbamate self-immolative unit: utilization for the targeted delivery of alcohol-containing payloads with antibody–drug conjugates. *Angew. Chem. Int. Ed.* **55**, 7948–7951 (2016).
31. Cramer, J., Sager, C. P. & Ernst, B. Hydroxyl groups in synthetic and natural-product-derived therapeutics: a perspective on a common functional group. *J. Med. Chem.* **62**, 8915–8930 (2019).
32. Dokter, W. et al. Preclinical profile of the HER2-targeting ADC SYD983/SYD985: introduction of a new duocarmycin-based linker-drug platform. *Mol. Cancer Ther.* **13**, 2618–2629 (2014).
33. Govindan, S. V. et al. Improving the therapeutic index in cancer therapy by using antibody–drug conjugates designed with a moderately cytotoxic drug. *Mol. Pharm.* **12**, 1836–1847 (2015).
34. Maneiro, M. A. et al. Antibody–PROTAC conjugates enable HER2-dependent targeted protein degradation of BRD4. *ACS Chem. Biol.* **15**, 1306–1312 (2020).
35. Kern, J. C. et al. Discovery of pyrophosphate diesters as tunable, soluble, and bioorthogonal linkers for site-specific antibody–drug conjugates. *J. Am. Chem. Soc.* **138**, 1430–1445 (2016).
36. Poudel, Y. B. et al. Design, synthesis and biological evaluation of phenol-linked uncialamycin antibody-drug conjugates. *Bioorg. Med. Chem. Lett.* **30**, 126782 (2020).
37. Iwata, T. N. et al. A HER2-targeting antibody–drug conjugate, Trastuzumab Deruxtecan (DS-8201a), enhances antitumor immunity in a mouse model. *Mol. Cancer Ther.* **17**, 1494–1503 (2018).
38. Zhang, Y. et al. Evaluation of double self-immolative linker-based antibody–drug conjugate FDA022-BB05 with enhanced therapeutic potential. *J. Med. Chem.* **67**, 19852–19873 (2024).
39. Park, S. et al. Sulfonate Version of OHPAS Linker has two distinct pathways of breakdown: elimination route allows Para-Hydroxy-Protected Benzylsulfonate (PHP-BS) to serve as an alternative self-immolative group. *Bioconjugate Chem.* **31**, 1392–1399 (2020).
40. Cortés, J. et al. Trastuzumab Deruxtecan versus Trastuzumab Emtansine for breast cancer. *N. Engl. J. Med.* **386**, 1143–1154 (2022).
41. Wang, X. et al. 42P safety, tolerability, pharmacokinetics, and anti-tumor activity of FDA022-BB05 in patients with advanced/metastatic solid tumors: a multicenter, open-label, first-in-human, phase I/Ib study. *Ann. Oncol.* **35**, S1420–S1421 (2024).
42. Mehellou, Y., Rattan, H. S. & Balzarini, J. The ProTide prodrug technology: from the concept to the clinic. *J. Med. Chem.* **61**, 2211–2226 (2018).
43. Serpi, M. & Pertusati, F. An overview of ProTide technology and its implications to drug discovery. *Expert Opin. Drug Discov.* **16**, 1149–1161 (2021).
44. Sofia, M. J. et al. Discovery of a β-d-2′-Deoxy-2′-α-fluoro-2′-β-C-methyluridine Nucleotide Prodrug (PSI-7977) for the treatment of hepatitis C Virus. *J. Med. Chem.* **53**, 7202–7218 (2010).
45. Lee, W. A. et al. Selective intracellular activation of a novel prodrug of the human immunodeficiency virus reverse transcriptase inhibitor tenofovir leads to preferential distribution and accumulation in lymphatic tissue. *Antimicrob. Agents Chemother.* **49**, 1898–1906 (2005).
46. Siegel, D. et al. Discovery and synthesis of a phosphoramidate prodrug of a Pyrrolo[2,1-f][triazin-4-amino] Adenine C-Nucleoside (GS-5734) for the treatment of ebola and emerging viruses. *J. Med. Chem.* **60**, 1648–1661 (2017).
47. Lackey, D. B. et al. Enzyme-catalyzed therapeutic agent (ECTA) design: activation of the antitumor ECTA compound NB1011 by thymidylate synthase. *Biochem. Pharmacol.* **61**, 179–189 (2001).
48. Slusarczyk, M. et al. Application of ProTide technology to gemcitabine: a successful approach to overcome the key cancer resistance mechanisms leads to a New Agent (NUC-1031) in clinical development. *J. Med. Chem.* **57**, 1531–1542 (2014).
49. Bré, J. et al. The novel anti-cancer fluoropyrimidine NUC-3373 is a potent inhibitor of thymidylate synthase and an effective DNA-damaging agent. *Cancer Chemother. Pharm.* **91**, 401–412 (2023).
50. Jin, H. et al. Thio-ProTide strategy: a novel H2S donor–drug conjugate (DDC) alleviates hepatic injury via innate lysosomal targeting. *Acta Pharm. Sin. B* **14**, 5341–5356 (2024).
51. Syed, Y. Y. Sacituzumab Govitecan: first approval. *Drugs* **80**, 1019–1025 (2020).
52. Kasper, M.-A. et al. Cysteine-selective phosphonamidate electrophiles for modular protein bioconjugations. *Angew. Chem. Int. Ed.* **58**, 11625–11630 (2019).
53. Kasper, M.-A. et al. Vinylphosphonites for Staudinger-induced chemoselective peptide cyclization and functionalization. *Chem. Sci.* **10**, 6322–6329 (2019).
54. Goldenberg, D. M., Sharkey, R. M., Govindan, S. V. & Cardillo, T. M. Novel peptide camptothecin drug-linkers for potent ADCs—Letter. *Mol. Cancer Therapeutics* **21**, 237–237 (2022).
55. Ochtrop, P. et al. Compact hydrophilic electrophiles enable highly efficacious high DAR ADCs with excellent in vivo PK profile. *Chem. Sci.* https://doi.org/10.1039/D2SC05678J (2023).
56. Staudacher, A. H. & Brown, M. P. Antibody drug conjugates and bystander killing: is antigen-dependent internalisation required? *Br. J. Cancer* **117**, 1736–1742 (2017).
57. Lhospice, F. et al. Site-specific conjugation of monomethyl Auristatin E to anti-CD30 antibodies improves their pharmacokinetics and therapeutic index in rodent models. *Mol. Pharm.* **12**, 1863–1871 (2015).
58. McGuigan, C. et al. Synthesis, anti-human immunodeficiency virus activity and esterase lability of some novel carboxylic ester-modified phosphoramidate derivatives of Stavudine (d4T). *Antivir. Chem. Chemother.* **9**, 473–479 (1998).
59. Balamkundu, S. & Liu, C. F. Lysosomal-cleavable peptide linkers in antibody-drug conjugates. *Biomedicines* **11**. https://doi.org/10.3390/biomedicines11113080 (2023).
60. Kuriki, Y. et al. Modular design platform for activatable fluorescence probes targeting carboxypeptidases based on protide chemistry. *J. Am. Chem. Soc.* **146**, 521–531 (2024).
61. Hamblett, K. J. et al. Effects of drug loading on the antitumor activity of a monoclonal antibody drug conjugate. *Clin. Cancer Res.* **10**, 7063–7070 (2004).
62. Andrikopoulou, A. et al. Trastuzumab Deruxtecan (DS-8201a): the latest research and advances in breast cancer. *Clin. Breast Cancer* **21**, e212–e219 (2021).
63. Caculitan, N. G. et al. Cathepsin B is dispensable for cellular processing of Cathepsin B-cleavable antibody–drug conjugates. *Cancer Res.* **77**, 7027–7037 (2017).
64. Ha, S. Y. Y. et al. An enzymatically cleavable tripeptide linker for maximizing the therapeutic index of antibody-drug conjugates. *Mol. Cancer Ther.* **21**, 1449–1461 (2022).
65. Proia, D. A. & Bates, R. C. Ganetespib and HSP90: translating preclinical hypotheses into clinical promise. *Cancer Res.* **74**, 1294–1300 (2014).
66. Park, I. W., Reddy, M. V. R., Reddy, E. P. & Groopman, J. E. Evaluation of novel cell cycle inhibitors in mantle cell lymphoma. *Oncogene* **26**, 5635–5642 (2007).

67. Koltai, T. et al. Resistance to gemcitabine in pancreatic ductal adenocarcinoma: a physiopathologic and pharmacologic review. *Cancers* **14**, 2486 (2022).
68. Janzer, A. et al. Abstract DDT02-04: BAY 2402234: a novel, selective dihydroorotate dehydrogenase (DHODH) inhibitor for the treatment of myeloid malignancies. *Cancer Res.* **78**, DDT02-04–DDT02-04 (2018).
69. Kuduk, S., Zhang, Z., Deratt, L. & Wang, A. Dihydroorotate dehydrogenase inhibitors. WO 2020/212897 A1. https://patentscope.wipo.int/search/en/detail.jsf?docId=WO2020212897 (2020).
70. Chandarlapaty, S. et al. SNX2112, a synthetic heat shock protein 90 inhibitor, has potent antitumor activity against HER kinase–dependent cancers. *Clin. Cancer Res.* **14**, 240–248 (2008).
71. Sharifi-Rad, J. et al. Paclitaxel: application in modern oncology and nanomedicine-based cancer therapy. *Oxid. Med. Cell. Longev.* **2021**, 3687700 (2021).
72. Zhao, G. et al. Discovery of a highly selective NAMPT inhibitor that demonstrates robust efficacy and improved retinal toxicity with nicotinic acid coadministration. *Mol. Cancer Ther.* **16**, 2677–2688 (2017).
73. Burke, P. J. et al. Novel immunoconjugates comprised of streptonigrin and 17-amino-geldanamycin attached via a dipeptide-p-aminobenzyl-amine linker system. *Bioorg. Med. Chem. Lett.* **19**, 2650–2653 (2009).
74. Shao, T. et al. Construction of paclitaxel-based antibody–drug conjugates with a PEGylated linker to achieve superior therapeutic index. *Signal Transduct. Target. Ther.* **5**, 132 (2020).
75. Wang, Z., Li, H., Gou, L., Li, W. & Wang, Y. Antibody–drug conjugates: recent advances in payloads. *Acta Pharm. Sin. B* **13**, 4025–4059 (2023).
76. Noble, S. & Goa, K. L. Gemcitabine. *Drugs* **54**, 447–472 (1997).
77. Zhang, Z. et al. Hypoxia potentiates gemcitabine-induced stemness in pancreatic cancer cells through AKT/Notch1 signaling. *J. Exp. Clin. Cancer Res.* **37**, 291 (2018).
78. Ciccolini, J., Serdjebi, C., Peters, G. J. & Giovannetti, E. Pharmacokinetics and pharmacogenetics of Gemcitabine as a mainstay in adult and pediatric oncology: an EORTC-PAMM perspective. *Cancer Chemother. Pharm.* **78**, 1–12 (2016).

Acknowledgements

The authors thank Danila Hauswald for excellent technical assistance in antibody purification. We also acknowledge the NMR facility at the Ludwig-Maximilians-Universität München (LMU) and its Head, Julian Holzinger, for providing access and support with NMR measurements. The study was funded by Tubulis GmbH.

Author contributions

P. O.: Data curation, Formal Analysis, Investigation, Methodology, Supervision, Writing—review & editing. A. P. J.: Data curation, Investigation, Writing—review & editing. J. G. F.: Data curation, Formal Analysis, Visualization, Writing—review & editing. S. V.: Investigation. I. M.: Data curation, Investigation. P. C.: Data curation. S. S.: Data curation, Formal Analysis, Supervision. S. P.: Data curation. A. K.: Data curation. S. W.: Investigation. P. M.: Data curation. J. B.: Data curation. S. H.: Data curation, N. L.: Data curation, E. P.: Data curation, C. P. R. Hackenberger: Writing—review & editing. O. M.: Supervision. D. S.: Funding acquisition, Project administration, Supervision. J. H.: Methodology, Funding acquisition, Project administration, Supervision. A. M. V.: Methodology, Supervision. M.-A. Kasper: Conceptualization, Data curation, Investigation, Methodology, Supervision, Visualization, Writing—original draft.

Competing interests

The authors declare competing financial interests: All authors, except from C. P. R. H are or have been full-time employees of Tubulis GmbH. The presented work is part of a pending patent application by J. H., D. S., P. O., A. P. J., S. V., S. W. and M.-A. K.

Additional information

Supplementary information The online version contains supplementary material available at https://doi.org/10.1038/s41467-026-68605-y.

Correspondence and requests for materials should be addressed to Marc-André. Kasper.

Peer review information *Nature Communications* thanks Thomas H. Pillow, Iman Kavianinia and the other anonymous reviewer(s) for their contribution to the peer review of this work. A peer review file is available.